

# Now you see it, now you don't - the circumstellar disk in the GRO J1008–57 system

M. J. Coe<sup>1</sup>, A.J. Bird<sup>1</sup>, A.B. Hill<sup>1</sup>, V.A. McBride<sup>1</sup>, M. Schurch<sup>1</sup>

J. Galache<sup>1,2</sup>, C. A. Wilson<sup>3</sup>, M. Finger<sup>3</sup>, D.A. Buckley<sup>4</sup> & E. Romero-Colmenero<sup>4</sup>

<sup>1</sup> *School of Physics and Astronomy, Southampton University, SO17 1BJ, UK*

<sup>2</sup> *Harvard-Smithsonian Center for Astrophysics, 60 Garden Street, Cambridge, MA 02138, USA.*

<sup>3</sup> *NASA/MSFC, Huntsville, AL 35812, USA*

<sup>4</sup> *South African Astronomical Observatory, P.O. Box 9, Observatory, 7935, South Africa.*

16 Apr 2007

## ABSTRACT

Multiwavelength observations are reported here of the Be/X-ray binary pulsar system GRO J1008–57. Over ten years worth of data are gathered together to show that the periodic X-ray outbursts are dependant on both the binary motion and the size of the circumstellar disk. In the first instance an accurate orbital solution is determined from pulse periods, and in the second case the strength and shape of the H $\alpha$  emission line is shown to be a valuable indicator of disk size and its behaviour. Furthermore, the shape of the emission line permits a direct determination of the disk size which is in good agreement with theoretical estimates. A detailed study of the pulse period variations during outbursts determined the binary period to be  $247.8 \pm 0.4$  d, in good agreement with the period determined from the recurrence of the outbursts.

**Key words:** stars:neutron - X-rays:binaries

## 1 INTRODUCTION AND BACKGROUND

The Be/X-ray systems represent the largest sub-class of massive X-ray binaries. A survey of the literature reveals that of the 115 identified massive X-ray binary pulsar systems (identified here means exhibiting a coherent X-ray pulse period), most of the systems fall within this Be counterpart class of binary. The orbit of the Be star and the compact object, presumably a neutron star, is generally wide and eccentric. X-ray outbursts are normally associated with the passage of the neutron star close to the circumstellar disk (Okazaki & Negueruela 2001). A review of such systems may be found in Coe et al. (2000).

The source that is the subject of this paper, the X-ray transient GRO J1008–57, was discovered on July 14 1993 by the BATSE experiment on the Compton Gamma Ray Observatory (Stollberg et al. 1993 and Wilson et al. 1994). The source was observed in the 20–200 keV band, and was found to be pulsating at a period of 93.5s. Its spectrum was observed to be consistent with optically thin thermal bremsstrahlung with  $kT=25$  keV. From these X-ray data it was concluded that the system was a massive binary system - a neutron star with either a Be or supergiant primary. A full report of this discovery outburst was presented in Shrader et al. (1999).

Subsequently the optical counterpart was identified by Coe et al, (1994) who showed it to be a  $V=15.3$  OB star with a strong IR excess and strong Balmer line emission. In this paper we present more than 10 years of optical monitoring of this counterpart, including a blue-end spectrum taken from the Southern African Large Telescope (SALT), which enables refinement of the spectral class to much higher accuracy than previous published work. We also demonstrate how the optical characteristics correlate with the long-term X-ray (RXTE/ASM data) behaviour. This is supplemented by  $\gamma$ -ray observations from INTEGRAL, in particular, reporting the details of the June 2004 outburst from GRO J1008–57.

## 2 OPTICAL DATA

### 2.1 Red spectra

H $\alpha$  data have been collected over the last 13 years from a series of telescopes. The dates and properties of the H $\alpha$  line are presented in Table 1. In this table the following telescopes and configurations have been used:

- AAT - 3.9m telescope, AAT (Australia), Royal Greenwich Observatory Spectrograph (RGOS), 25cm camera,

**Table 1.** Table of H $\alpha$  measurements. See text for details of observatory/instrument used.

Observation Date	Observatory	H $\alpha$ EW ( $\text{\AA}$ )	Peak Separation ( $\text{km s}^{-1}$ )
21 Dec 1993	SAAO	-17 $\pm$ 2	
24 Dec 1993	SAAO	-13.6 $\pm$ 1.3	250
26 Feb 1994	AAT	-19.4 $\pm$ 1.2	215
07 Mar 1994	SAAO	-19.6 $\pm$ 0.5	
26 Feb 1995	SAAO	-19 $\pm$ 3	
19 Nov 1995	SAAO	-11 $\pm$ 2	
20 Jun 1997	SAAO	-2.6 $\pm$ 1.5	
20 Jun 1997	SAAO	-4.9 $\pm$ 1.3	350
06 Feb 1998	SAAO	-6.7 $\pm$ 1.2	
11 Jan 1999	SAAO	-19.0 $\pm$ 1.6	
14 Dec 2002	SAAO	-20 $\pm$ 2	
15 Mar 2005	SAAO	-22.6 $\pm$ 1.7	
19 Mar 2005	SAAO	-21.5 $\pm$ 1.5	243
07 May 2006	SAAO	-20.9 $\pm$ 1.2	

1200V grating and TEK (1024x1024) CCD. The dispersion was 0.8 $\text{\AA}$ /pixel and the signal to noise ratio from the 600s exposure was  $\sim$ 40.

- SAAO - 1.9m telescope, Sutherland Observatory (South Africa), spectrograph, SITe detector, 1200 l/mm grating. The dispersion was 1.0 $\text{\AA}$ /pixel and the signal to noise ratio  $\sim$ 10.

Selected H $\alpha$  line profiles are presented in Figure 1, where more than one spectra exists for a particular year then an average of the two is shown. A clear evolution of the Balmer line over the 10 year period is seen. Apart from the structural changes which will be discussed below, the strength of the H $\alpha$  emission line varies considerably over the  $\sim$ 10 year period - see Figure 2. The equivalent width determinations can be seen to go through a significant decline in the middle of the period, recovering strongly in the latest data.

The peak separations were determined by fitting Lorentzian profiles to the H $\alpha$  emission lines. In the cases where the  $\chi^2$  was significantly improved by including two lines, as opposed to one line, the line parameters were used to measure the separation (in velocity space) between the red and violet peaks. These kind of changes in the line profiles are common in Be stars (see, for example, Telting & Kaper 1994).

## 2.2 Blue spectrum

A blue end spectrum was obtained from SALT on 18 June 2006 - see Figure 3. The spectrum was obtained using the Robert Stobie Spectrograph in long slit mode, with a grating resolution of 1800 l/mm and an exposure time of 600s. This gave a dispersion of 0.34 $\text{\AA}$ /pixel and a signal to noise varying from  $\sim$ 10 (blue end) to  $\sim$ 50 (red end).

Mosaicking of the three chips was performed by using the SALT IRAF packages (the two chip gaps are clearly visible in Figure 3) as part of the pipeline processing of the data. Further wavelength calibrations were performed using an Ar arc lamp solution. No flux calibration has been made. The prominent feature is the strong double peaked H $\beta$

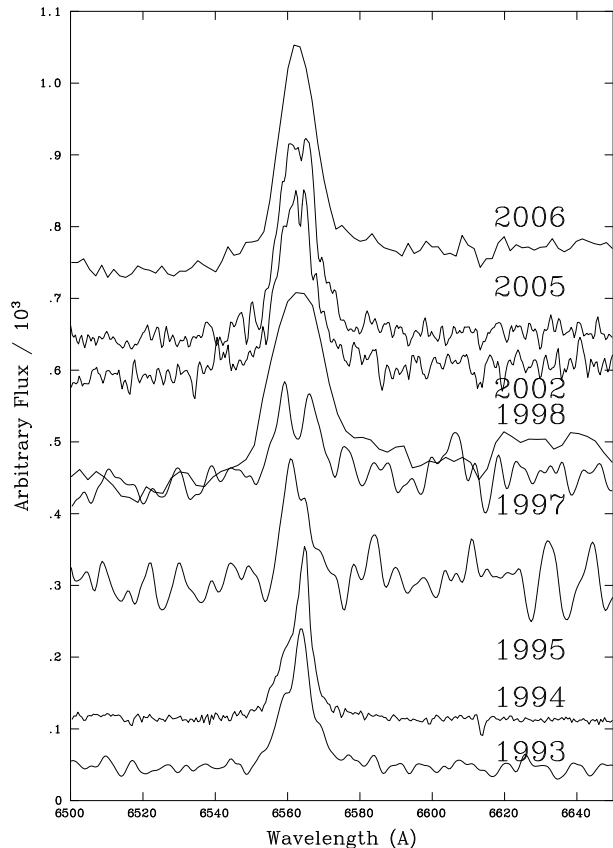


**Figure 1.** The evolution of the H $\alpha$  profile over 13 years. Individual spectra have been arbitrarily re-scaled in flux to permit the shape of the H $\alpha$  profile to be clearly visible.

line, which has an equivalent width of  $-1.74 \pm 0.09\text{\AA}$ . The only previous blue end spectrum (Coe et al.1994) gives a H $\beta$  equivalent width of  $-1.4 \pm 0.1\text{\AA}$ . Two other Balmer lines (H $\gamma$  and H $\epsilon$ ) are visible; but H $\delta$  seems to have been effectively lost due to infilling. This is unusual given that the Balmer lines on either side do not seem to be so affected. The spectrum has been carefully checked for any evidence of scattered light or other instrument artefacts, but no evidence for any such features were found. The lack of any identifiable HeII lines, in particular 4686 $\text{\AA}$  indicates that the star is B1 or later (Walborn and Fitzpatrick 1990). Furthermore the presence of the OII CIII blend at 4650 $\text{\AA}$  restricts the classification to the range B1-B2 (Walborn and Fitzpatrick 1990). It is worth noting, however, that the lack of other metal lines is a little surprising but may be due, in part, to the decreasing signal-to-noise ratio towards the blue end of the spectrum. However, such a lack of lines is not uncommon in low metallicity environments such as the Small Magellanic Cloud (McBride et al, 2007).

## 3 ORBITAL X-RAY PROFILE

X-ray monitoring data were collected by the All Sky Monitor (ASM) instrument on the Rossi X-ray Timing Explorer (RXTE) observatory. The data consist of daily flux averages covering the X-ray energy range 1.3 – 12.1 keV. There

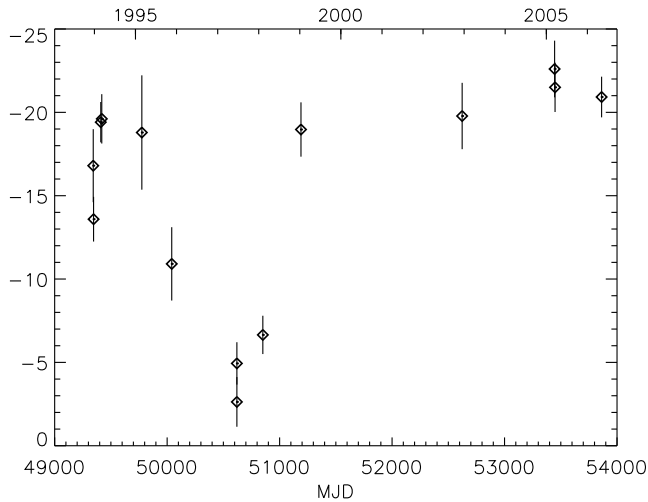


**Figure 2.** The evolution of the flux of the H $\alpha$  emission line over 13 years (1993–2006).

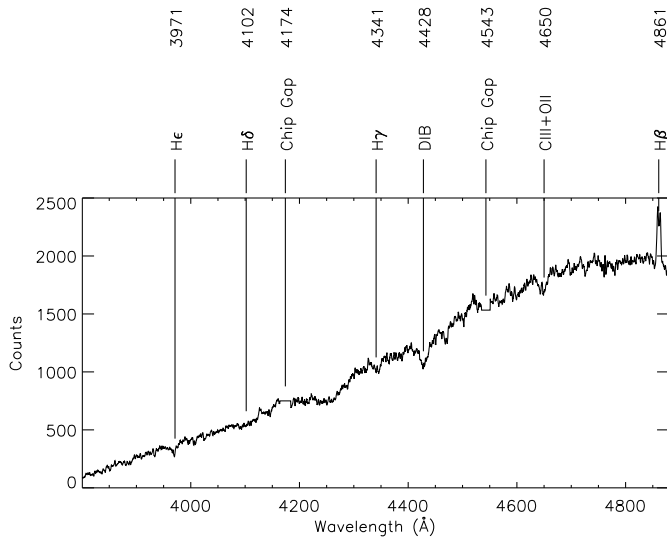


**Figure 3.** SALT blue spectrum of the optical counterpart to GRO J1008-57. Major features in the spectrum are indicated.

is no evidence in the daily data averages for any significant detection of the source on short timescales ( $\sim$  a few days).

The  $\sim$ 10 years worth of data were folded at the proposed binary period of 248.9d determined by Levine & Corbet, 2006 from the same data. A strong, clear modulation at that period is very obvious.

Since it is clear from Figure 2 that the strength of the H $\alpha$  line has been significantly changing over the 10 year interval of the ASM data, the complete data set was divided into two equal periods (1996-2001 & 2001-2006). Each data set was separately folded at this same period and with the same phase. The results are shown in the lower two panels of Figure 4 from which it is clear that the degree of modulation had changed very significantly over the 10 years.

To explore the modulation at even earlier times (i.e. before 1996) data from the BATSE occultation instrument on Compton Gamma Ray Observatory (CGRO) were folded

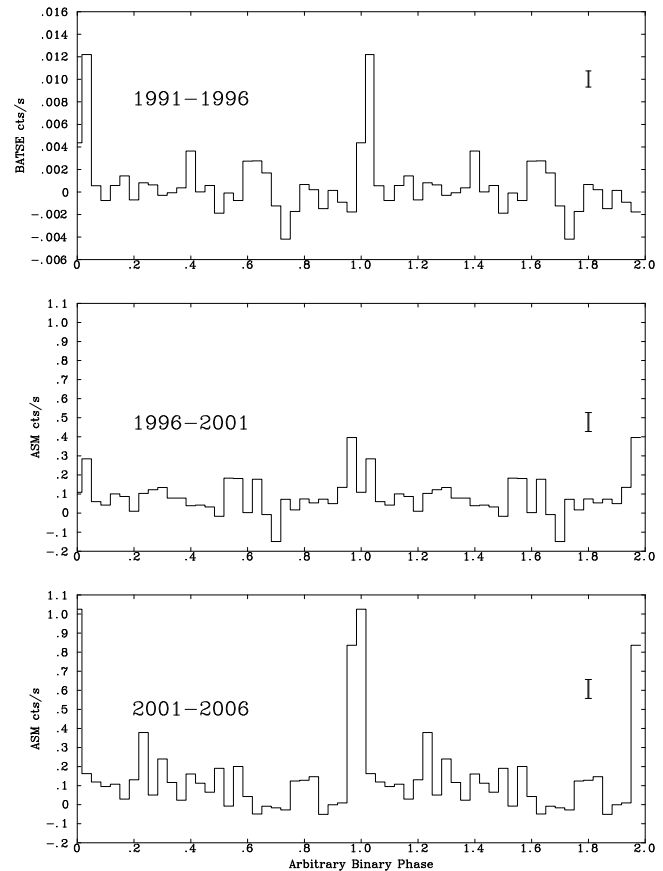


**Figure 4.** BATSE (top panel) and RXTE/ASM (lower two panels) data folded at the period of 248.9d (Levine & Corbet, 2006) for three different time intervals. The phases shown are those corresponding to the ephemeris given in Section 6.1. In each case a  $\pm 1\sigma$  error bar is shown.

at the same period and same phase. These data cover the harder spectral range of 20 – 100 keV, but reveal a very similar modulation occurring in the period 1991-1996 - see upper panel in Figure 4. The phase of the outburst and the degree of modulation looks very similar to that seen with RXTE/ASM in recent years.

#### 4 CGRO/BATSE ORBITAL SOLUTION

The data types that are available from the 8 BATSE detectors on CGRO are the 16-channel continuous or “CONT” data, sampled at 2.048s intervals, and the 4-channel discriminator or “DISCLA” data sampled every 1.024s. For the analyses in the present work the DISCLA data were used from which pulsed fluxes and frequencies were extracted (see Bildsten et al.1997 for a full explanation on the use of DISCLA data for pulsar observations).

To assess the confidence in the detection of a known pulsar, the data were searched through in a narrow frequency range centred on the pulsar’s nominal frequency.

First the DISCLA rates were grouped into 300 s intervals. A pulse profile was then estimated using a 6th order Fourier expansion for each of these intervals. These profiles were then grouped into 4-day intervals. Within each 4-day

interval, the Fourier coefficients for each 300-s pulse profile were re-computed for a grid of offsets from the nominal frequency. The best frequency offset was determined using the  $Z_n^2$  statistic (Buccheri 1983), expressed as:

$$Z_n^2 = \sum_{k=1}^N \frac{|\mu_{k_{min}}|^2}{\sigma_{\mu_k}^2} \quad (1)$$

where  $\mu_{k_{min}}$  are the mean Fourier coefficients and  $\sigma_{\mu_k}$  their Poisson errors;  $N$  can take any value from 1 to 6 (in general  $N = 3$  or 6 was used). In addition, within each 4-day interval, a mean pulse profile was determined for each frequency offset by chi-square minimization. Unfortunately, BATSE noise is generally non-Poissonian (Bildsten et al. 1997), so  $\sigma_{\mu_k}$  is multiplied by the reduced chi-square factor to produce the new statistic  $Y_n$ . Monte-Carlo methods are required to convert  $Y_n$  into percentile significances in order to establish confidence levels for the detected signal. An advantage to using this method is that any number of harmonics can be excluded from the statistic if there are other sources within the field of view with pulsations at those particular harmonic frequencies.

If an outburst lasts for a significant fraction of a system's binary orbital period, the size and shape of the orbit can be determined by analysing Doppler shifts and pulse arrival delays in the pulsar signal. As an outburst progresses, BATSE obtains a continuous history of the daily source intensity and frequency; this detected frequency will be the intrinsic spin frequency of the pulsar plus or minus a shift due to the neutron star's orbit around its companion. The process of calculating the orbit is further complicated by the fact that the neutron star is usually spinning up or down during an outburst, and so it is necessary to disentangle the orbital from the spin torque effects.

The method used with the BATSE data is the piecewise approach explained in detail in Wilson et al, 2003. In essence, it assumes that the torque during an outburst will be approximately constant during small time intervals, such that the intrinsic spin up will be linear during this time. As such, the data available during an outburst will be divided into short segments of 3–5 data points each. In order to compute the orbital parameters of the system, the data in all the segments are fitted with global values of  $P_{orb}$ ,  $\tau_p$ ,  $e$ ,  $\omega$  and  $a_x \sin i$ , but a different  $\nu_{intr}$  in each segment.

GRO J1008–57 was first detected during a bright outburst in July 1993 by BATSE with pulsations at  $93.587 \pm 0.005$ s (Stollberg et al, 1993). This outburst can be seen around JD 2449200 in the second from top panel in Figure 5. After this initial outburst, a number of less significant detections were made, which could correspond to 5 further outbursts. These are spaced  $\sim 260$ d apart, which led to this being proposed as the orbital period of the system (Finger et al.1994). Shrader et al. (1999) find weak evidence for a  $\sim 135$ d period in the ASM data from RXTE.

Orbit fitting calculations were carried out using the  $\geq 99.9\%$  significance data points (all the points illustrated in Figure 5), producing an orbital period of  $247.8 \pm 0.4$ d. This is in good agreement with the Levine & Corbet (2006) value of  $248.9 \pm 0.5$ d. The results can be seen graphically in Figure 5 and the orbital parameters are presented in Table 2.

Using the frequencies corrected for orbital motion from Figure 5 we derive for the initial outburst a  $\dot{P} = -5.6 \times$

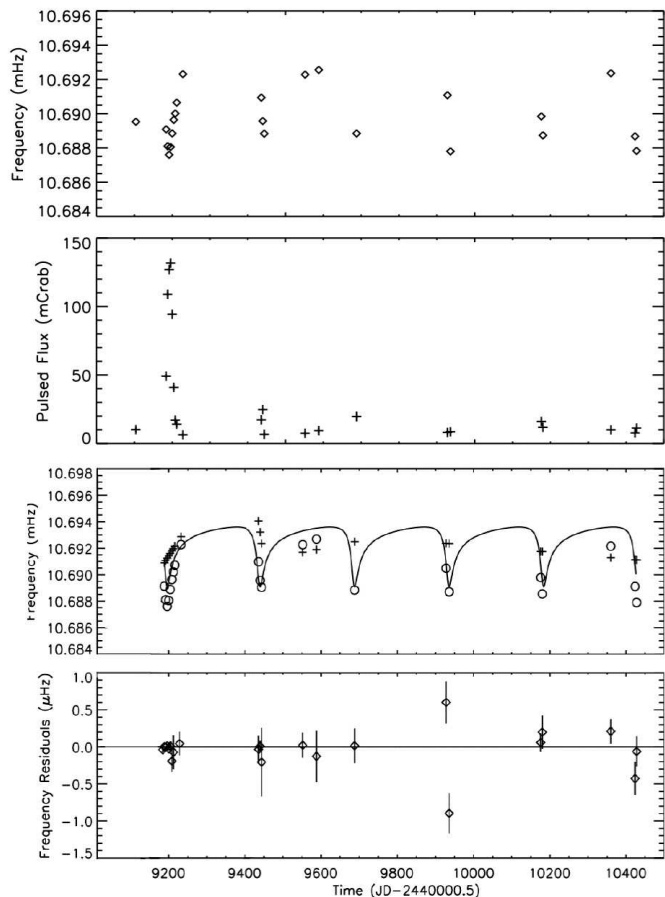


**Figure 5.** BATSE data of GRO J1008–57. Top panel shows 4-day averaged frequencies and the second panel down shows the pulsed flux (n.b. only the  $Y_n \geq 99.9\%$  significance data points are shown). Third panel: the crosses are the emitted frequency returned by fitting the model described in the text; the solid line illustrates the magnitude of the orbital effect and the circles are the frequencies as measured by BATSE. Lowest panel : pulse frequency residuals for the model.

**Table 2.** Orbital parameters for GRO J1008-57.

$P_{orbital}$ (d)	$247.8 \pm 0.4$
$e$	$0.68 \pm 0.02$
$a_x \sin i$ (light-s)	$530 \pm 60$
$\tau_{periastron}$ (MJD)	$49189.8 \pm 0.5$

$10^{-9} \text{ss}^{-1}$  implying  $L_x = 1.0 \times 10^{36} \text{erg s}^{-1}$  ( $B = 1.4 \times 10^{13} \text{G}$ ). Compare to  $L_x = 4.1 \times 10^{36} \text{erg s}^{-1}$  ( $B = 6.0 \times 10^{13} \text{G}$ ), obtained by Shrader et al. 1999.

## 5 INTEGRAL $\gamma$ -RAY DATA

GRO J1008–57 was detected by INTEGRAL on two occasions - June 2004 and October 2005 (Grebenev et al., 2005 have reported on the latter outburst). On many other occasions the source has fallen within the INTEGRAL field of view. The data from the IBIS imaging instrument on-board

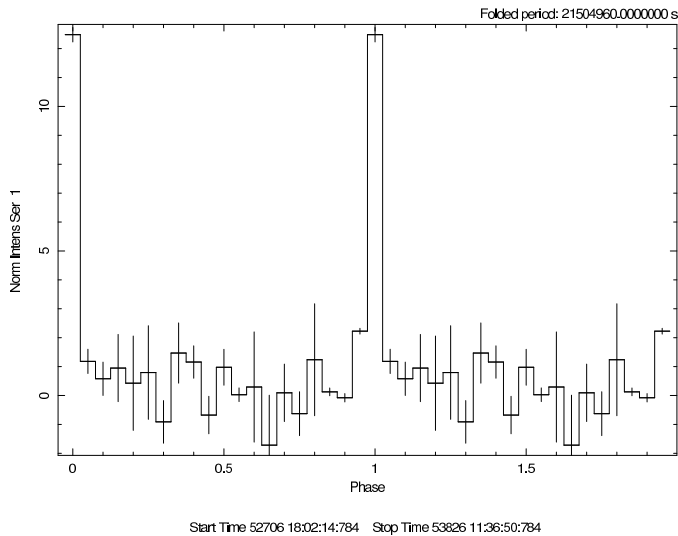


**Figure 6.** All available INTEGRAL data in 18-60 keV range folded at the outburst period of 248.9d. The phase is the same as in Figure 4.

INTEGRAL were reduced and analysed using the standard *Offline Science Analysis, OSA*, software version 5.1.

A light curve was obtained by analysing all available INTEGRAL data when the source was within the IBIS/ISGRI field of view (1085 science windows) and extracting the 18-60 keV flux at the source position in each science window. The sampling time for this light curve is therefore at the typical science window duration of  $\sim 2000$ s. Folding the light curve on the ephemeris given in Section 6.1 yields the folded light curve shown in Figure 6. Though the modulation shown is dominated by the one major outburst of June 2004 the profile is in good phase agreement with that shown in Figure 4 for the BATSE and RXTE/ASM outbursts.

Since there are not many data on the second outburst, the results from the first, previously unreported outburst are presented in this section.

A lightcurve of the 2004 outburst is shown in Figure 7 for the photon energy range 18-60 keV. From this figure it is possible to ascertain that the main burst lasted less than 23.5 days, and rose in an approximately linear manner with a doubling time of  $\sim 3.5$ d. In total INTEGRAL observed this outburst for  $\sim 7.9$  d.

A 10s binned light curve in the 20-40 keV photon energy range was obtained from the IBIS/ISGRI data using the *OSA ii\_light* tool. The finely binned lightcurve was analysed using the Lomb-Scargle periodogram method by means of the fast implementation of Press & Rybicki (1989). The resulting power spectrum shows a clear strong peak at 0.01068 Hz with a power of  $\sim 435$ . Using the error formulae derived by Horne & Baliunas (1986) we find that this corresponds to a periodicity of  $93.6672 \pm 0.0005$ s. This period was independently confirmed by the 4-10 keV data from the X-ray camera on-board INTEGRAL, JEM-X. Furthermore, the period is in very close agreement to that of  $93.62 \pm 0.01$  reported by Shrader et al. (1999) from the 1993 ASCA data, indicating very little spin up (or down) over more than a decade.

The phase folded pulse profile was determined in 4 sep-

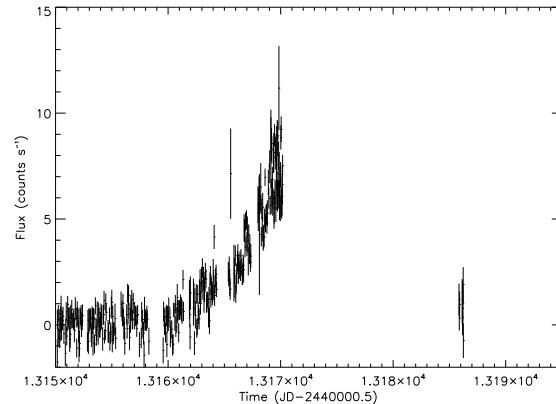


**Figure 7.** INTEGRAL IBIS data showing the outburst of June 2004 in the energy range 18-60 keV.

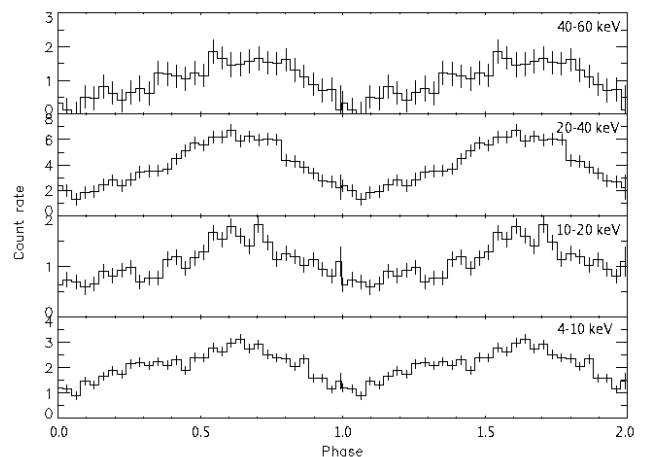


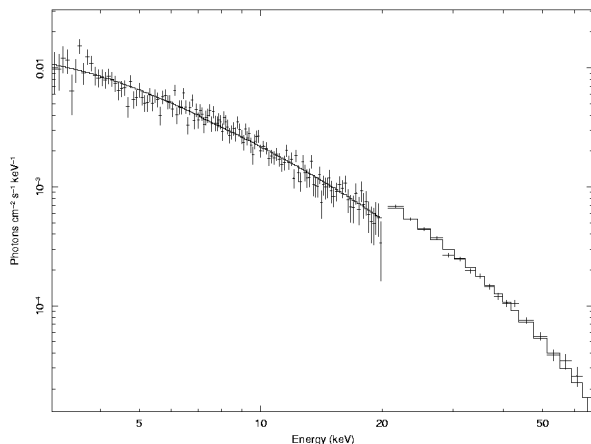
**Figure 8.** INTEGRAL IBIS and JEM-X pulse profiles.

arate energy channels; 4-10 and 10-20 keV from JEM-X and 20-40 and 40-60 keV from IBIS/ISGRI. The resulting single peaked profiles are shown in Figure 8. From these profiles it was possible to determine the pulse fractions,  $(I_{max} - I_{min})/I_{max}$ , to be  $72 \pm 8\%$  in the 4-10 keV band,  $70 \pm 10\%$  in the 10-20 keV band,  $80 \pm 10\%$  in the 40-60 keV, and  $100 \pm 30\%$  in the 40-60 keV range. The IBIS/ISGRI pulse fractions must be treated with care as they are derived from the folded fine timing lightcurve and consequently are not absolutely flux calibrated.

Spectra for the 2004 outburst of GRO J1008-57 were produced using OSA for both the IBIS/ISGRI and JEM-X instruments. The source was not always within the field of JEM-X and consequently there were only 12 science windows of data available spread across the outburst where the source was detected by that instrument. The IBIS/ISGRI data for the same time span comprised of  $\sim 80$  science windows. The spectra were fit simultaneously in *XSPEC 12.3.0*; the JEM-X data were fit over the 3-20 keV range and the IBIS/ISGRI data over the 20-100 keV range. A cross-calibration constant,  $C_{ISGRI}$ , was added to all spectral models to account

**Table 3.** The results of the simultaneous spectral fits of the JEM-X and ISGRI data.

Parameter	Cut-off Power Law	Thermal Bremsstrahlung
$C_{ISGRI}$	$1.6 \pm 0.1$	$1.5 \pm 0.1$
cut-off energy	$8.0 \pm 1.0$ keV	-
Fold energy	$21 \pm 2$ keV	-
Photon index	$1.4 \pm 0.1$	-
kT	-	$21 \pm 1$ keV
$\chi^2/\text{dof}$	150.46/146	162.31/148

**Figure 9.** INTEGRAL combined IBIS and JEM-X spectrum obtained by deconvolving the data using the Cut-off Power Law model.

for any uncertainties in the matching of the two instruments. A systematic error of 2% was used.

Two spectral models were fit to the data, a power-law with a high energy cut-off and a thermal bremsstrahlung model. Both models fit equally well and have a reduced chi-square of  $\sim 1$ ; the details of the fit parameters are shown in Table 3. An attempt was made to introduce an absorption component to both, however the fit could not reasonably constrain the parameter. Consequently, an absorption component fixed to the anticipated galactic absorbing column density of  $\sim 1.5 \times 10^{22}$  cm $^{-2}$  was added. The unfolded spectra with the high-energy cut-off power law model fitted is shown in Figure 9.

The fluxes given by the spectral models were  $5.7 \times 10^{-10}$  erg cm $^{-2}$  s $^{-1}$  in the 3–20 keV band and  $4.1 \times 10^{-10}$  erg cm $^{-2}$  s $^{-1}$  in the 20–100 keV band. Taking these numbers combined with the source distance of 5kpc (Coe et al, 1994) produces a flux estimate of  $(1-2) \times 10^{36}$  erg s $^{-1}$ . This value is in good agreement with the level of X-ray luminosity estimated from the small accretion-torque driven pulse period changes reported in Section 4.

## 6 DISCUSSION

### 6.1 X-ray outburst ephemeris

Using the clear outburst profile presented in Figure 4 for the period 2001–2006 it is possible to determine an accurate ephemeris. We assume the binary period is 248.9d (Levine & Corbet, 2006) and chose the highest bin in the figure to

be defined as phase 0.0. From this the following outburst ephemeris is determined:

$$T_{\text{outburst}} = 50186 \pm 4 + 248.9n$$

where the dates are in Modified Julian Day format and  $n$  is the outburst number.

If the time of outburst is compared to the predicted time of periastron determined from the pulse period variations (see Table 2), it agrees within 1.5d for the MJD 49189 outburst, indicating no significant phase shift between these two events.

If we use this RXTE/ASM ephemeris then we can determine that the phase of the two INTEGRAL outbursts discussed here are 0.99 and 0.00. Furthermore, the phase of the peak of the 1993 BATSE outburst reported in Shrader et al. (1999) is 0.01. Thus all three reported events fit very comfortably with the above ephemeris and hence are almost certainly Type I outbursts. This is supported by comparing the phase of the peaks of outbursts as seen in the folded lightcurves from BATSE, RXTE/ASM and INTEGRAL all of which seem to match very well. There is no evidence for the phase changes in outburst seen in EXO 2030+375 and explained by Wilson et al. (2002) as related to global one arm oscillations in the circumstellar disk. Though there are changes in the disk, evidenced by the overall shape changes of the H $\alpha$  profile seen in Figure 1, they are obviously not great enough to result in such outburst phase shifting.

### 6.2 Determining the circumstellar disk size and its relationship to X-ray activity.

Figure 2 shows the H $\alpha$  equivalent width measurements over the last 13 years. Although the H $\alpha$  equivalent width is not a direct measurement of the size of the circumstellar disk the data in this figure can be used as an indicator of growth and decline in the disk. To this effect we interpret the significant decline in the H $\alpha$  flux, followed by a strong recovery as a period of disc shrinking and regrowth. This idea is consistent with the lack of observed X-ray outbursts of GRO J1008–57 during 1996–2001 - see Figure 4.

Another feature to take note of in Figure 2 is the maximum measured H $\alpha$  equivalent width. Reig, Fabregat & Coe (1997) show that this maximum H $\alpha$  equivalent width is correlated with the orbital period in a Be/X-ray binary and the observed correlation can be explained by a viscous circumstellar disk truncated by the resonant torque of the orbiting neutron star (Negueruela et al., 2001). The system under discussion here spends a large fraction of the observed timescale at an H $\alpha$  equivalent width of close to  $-20\text{\AA}$ , while undergoing Type I X-ray outbursts. This may suggest that the  $-20\text{\AA}$  EW measurement describes the circumstellar disk at a size that puts it close to the  $L_1$  point at periastron.

To estimate the size of the H $\alpha$  emitting region of the circumstellar disk we make use of the peak separation measurements in Table 1 and the relation from Huang (1972).

where  $r$  is the disk radius,  $i$  is the inclination and  $\Delta V$  is the peak separation. The average of the three measurements taken while the system was in normal outburst was determined to be  $236 \pm 15$  km/s and used in the following determination of the disk size.

From the blue spectrum we determine the spectral type of the optical counterpart of GRO J1008–57 to be B1 - B2 Ve. From Allen (1973) we estimate the mass and radius of

such a star to be  $15 M_{\odot}$  and  $7 R_{\odot}$  respectively. Then, using the measured values of  $a_x \sin i$  and assuming that the Be star disk is in the plane of the orbit we find an inclination angle of  $i = 36^{\circ}$  for the circumstellar disk of GRO J1008–57. These stellar parameters give an estimated  $H\alpha$  disk size of  $72 R_{\odot}$  and a ratio of disk size to  $L_1$  point (measured from the centre of the Be star) of  $R_d/R_L \sim 0.64$

In comparison, if the data for 1997 are used with a  $\Delta V$  of 350 km/s, then this results in a much smaller disk of the order of  $33 R_{\odot}$  in size.

Even the  $72 R_{\odot}$  is much smaller than the truncation radius predicted by the viscous disk theory for this Be/X-ray binary by Okazaki & Negueruela (2001). Using slightly different stellar and orbital parameters those authors predict that the circumstellar disk of GRO J1008-57 is most likely truncated at the 7:1 or 8:1 resonance radius. At such a radius the disk verges on the  $L_1$  point at periastron, thus explaining the frequently observed Type I outbursts.

Exploring the upper and lower limits of the disk size estimates presented in this work requires the identification of the major uncertainties affecting the results. The uncertainty in the spectral types introduces a range of possible masses for the Be star of  $10 - 18 M_{\odot}$ . Using extreme upper limits for both the stellar mass and  $a_x \sin i$ , with the lower limit on  $\Delta V$ , we find that  $R_d/R_L \sim 0.86$ . At the other end of the range we find  $R_d/R_L \sim 0.51$

However, it is worth bearing in mind that, contrary to the assumption in most disk models, the Be star disk is probably not isothermal. Thus the physical size of the disk is not constrained to the  $H\alpha$  emitted size of the disk. For example, in the case of the isolated Be star  $\Psi$  Per the  $H\alpha$  disk size has been measured by direct interferometry to be around ten stellar radii (Quirrenbach et al., 1997), whereas similar radio observations (Dougherty & Taylor 1992) suggest that material may be present as far away as hundreds and even thousands of stellar radii. So, in the case of GRO J1008–57 the totality of the disk may extend beyond the radius measured here from the  $H\alpha$  data. This is indirectly confirmed by the very fact that we see regular X-ray outbursts, suggesting the disk material must, indeed, reach the  $L_1$  point.

## 7 CONCLUSIONS

The study of pulse period changes in GRO J1008–57 from the BATSE data have allowed a precise orbital determination. The orbital period found agrees, within errors, with that determined by Levine & Corbet (2006) from X-ray outburst cycles. These outbursts seem to be very reliable in nature, showing no variation with X-ray energy, nor are they correlated with the changes in the  $H\alpha$  profile, as was seen in the case of EXO 2030+375 (Wilson et al, 2002). However, the substantial changes in the  $H\alpha$  EW correlate nicely with the existence and changing levels of the X-ray outburst sizes. In addition, using the peak separation measured from the  $H\alpha$  profiles an indication was provided of the disk size which is in general agreement with the detailed models of Okazaki & Negueruela (2001). The results are a direct confirmation of the value of multiwavelength observations of these complex systems.

## 8 ACKNOWLEDGEMENTS

This paper uses observations made from the South African Astronomical Observatory (SAAO), and X-ray data provided by the ASM/RXTE team. VAM acknowledges support from the South African NRF and the British Council in the form of a SALT/Stobie studentship.

## REFERENCES

- Allen, C.W. ‘Astrophysical Quantities’ 1973 Athlone Press.  
 Bildsten L. et al. 1997 ApJS 113, 367.  
 Buccheri R. et al. 1983 A&A 128, 245.  
 Coe, M.J. et al., 1994 MNRAS 270, L57.  
 Coe M.J. 2000 in “The Be Phenomenon in Early-Type Stars”, IAU Colloquium 175, ASP Conference Proceedings, Vol. 214, ed: M. A. Smith H. F. Henrichs. Astronomical Society of the Pacific, p.656.  
 Dougherty, S. M. and Taylor, A. R., 1992, Nature 359, 808.  
 Finger M.H., Wilson R.B., Scott M., Stollberg M. & Prince T.A. 1994 IAUC 5959, 2.  
 Gies, D.R. et al., 2007, ApJ 654, 527.  
 Grebenev S.A. et al., 2005, ATEL 647.  
 Grundstrom, E. D. and Gies, D. R. 2006, ApJL 651, L53.  
 Horne, J. H. & Baliunas, S. L., 1986, ApJ, 302, 757  
 Huang S. S., 1972, ApJ 171, 549.  
 Levine, A.M. & Corbet, R.H.D. 2006 ATEL 940.  
 McBride V., et al. 2007 (in prep).  
 Negueruela, I., Okazaki, A. T., Fabregat, J., Coe, M. J., Munari, U. and Tomov, T., 2001, A&A 369, 117.  
 Okazaki A.T. & Negueruela I., 2001, A&A 377, 161.  
 Press, W. H. & Rybicki, G. B., 1989, ApJ, 338, 277P.  
 Quirrenbach, A., Bjorkman, K. S., Bjorkman, J. E., Hummel, C. A., Buscher, D. F., Armstrong, J. T., Mozurkewich, D., Elias, N. M. and Babler, B. L. 1997, ApJ, 479, 477.  
 Reig P., Fabregat J. & Coe M.J. 1997, A&A, 322, 193.  
 Shrader, C.R., Sutaria, F.K., Singh, K.P. and Macomb D.J. 1999 ApJ 512, 920.  
 Stollberg M.T. et al., 1993, IAU Circular, 5836  
 Telting J.H. & Kaper L. 1994 A&A 284, 515.  
 Walborn N.R. and Fitzpatrick E.L. 1990 PASP 102, 379.  
 Wilson R.B. et al. 1994 *Evolution of X-ray Binaries*, Holt, S. & Day, C.S. (Eds), AIP Conference Proceedings 308, 451.  
 Wilson C.A., Finger M.H., Coe M.J., Laycock S. & Fabregat J., 2002, ApJ 570, 287.  
 Wilson C.A., Finger M.H., Coe M.J. & Negueruela I., 2003, ApJ 584, 996.

This paper has been typeset from a  $\text{T}_{\text{E}}\text{X}/\text{L}^{\text{A}}\text{T}_{\text{E}}\text{X}$  file prepared by the author.